Impact of VSC Control Strategies and Incorporation of Synchronous Condensers on Distance Protection under Unbalanced Faults

Jia, Jundi; Yang, Guangya; Nielsen, Arne Hejde; Rønne-Hansen, Peter

Published in:
IEEE Transactions on Industrial Electronics

Link to article, DOI:
10.1109/TIE.2018.2835389

Publication date:
2018

Document Version
Peer reviewed version

Impact of VSC Control Strategies and Incorporation of Synchronous Condensers on Distance Protection under Unbalanced Faults

Jundi Jia, *Student Member, IEEE*, Guangya Yang, *Senior Member, IEEE*,
Arne Hejde Nielsen, *Senior Member, IEEE*, and Peter Rønne-Hansen

***Abstract*—The short circuit response of a voltage source converter (VSC) under grid unbalanced faults mainly depends on the design of its control system. Due to the limited semiconductor overload capability, the short circuit current contributed by a VSC should be restricted within the limit for each phase. This might bring up challenges to the protection system of a converter-dominated power system. This paper derives a generic converter peak current limitation method for three different VSC control strategies. The impact of the control strategies and the combined impact of a VSC with a synchronous condenser on distance protection are evaluated using a commercial relay through hardware-in-the-loop (HIL) tests. Based on the test results, we propose to avoid using constant reactive power control strategy. It poses an adverse impact on the reliability and speed of distance protection regardless of the presence of SC at the point of common coupling (PCC), while constant active power and balanced current control strategies favor the performances of distance protection.**

***Index Terms*—Converter, distance protection, short circuit current, synchronous condensers, unbalanced faults.**

I. Introduction

As a concern of the worldwide climate change and growing demands for electricity, the integration of renewable energy into power systems has gained increasing attention. For example, Denmark aims to achieve 100% renewable energy supply by 2050, eliminating the dependency on fossil fuels [1]. This has led VSC-based sources (e.g., Type-IV wind power plants, photovoltaic power plants, HVDC transmissions) up to several hundred megawatts to be connected to the high-voltage transmission network.

However, the control system of a VSC is sensitive to grid disturbances such as unbalanced faults. The negative-sequence voltage appearing at the PCC will propagate in the VSC system affecting its control variables and hence its output [2]. If the control system is not designed properly, undesirable performances such as output voltage and current distortions, DC-link voltage oscillations and output power oscillations can be observed. This may even result in an undesirable trip of the converter. As transmission system operators (TSOs) have imposed strict requirements on converter-based sources such as fault-ride-through (FRT) and voltage support capability, a variety of control strategies based on symmetrical components have been proposed to improve VSC performances under unbalanced conditions. In [3]–[7], the control strategies are developed based on the objectives of achieving balanced current injection, minimization of DC voltage ripples or nullifying oscillations in either active or reactive powers. Generally, the above control strategies can be regarded as different special cases of [8], where flexible scalars are introduced to form the current references to flexibly control the oscillations in the active and reactive powers. In [9], the relative relationship between the positive- and negative-sequence powers can be flexibly adjusted. Based on [9], the studies in [10]–[12] regulate the grid phase voltages complying to predefined boundaries and [13] focuses on the effectiveness of unbalanced voltage compensation. With converter current restricted in each phase, [14] and [15] aim to maximally use the power capability of the converter under unbalanced faults. Therefore, the short circuit response of a VSC can be significantly different from each other under unbalanced faults and which control strategy is more suitable is still under open discussion.

Distance protection is widely utilized in high-voltage transmission networks and a variety of studies has been conducted regarding the impact of VSCs on distance protection. The speed of distance relays subject to balanced faults is evaluated by simulations in [16], where different fault types and penetration levels of renewable generation are examined. In [17], distance relays may refuse to trip when there is not enough fault current under balanced faults and communication-aided protection is suggested to overcome this problem. According to [18], the control action of VSCs may cause an underreaching problem for the backup distance protection located on adjacent lines. However, the studies mentioned above neither discuss unbalanced faults nor test on a real distance relay. Even though unbalanced faults are of interests in [19]–[24], none of them has considered the impact of different VSC control strategies incorporating a converter current limit in each phase.

Manuscript received July 22, 2017; revised November 10, 2017, January 19, 2018 and April 8, 2018; accepted May 1, 2018. This work was supported by the Danish ForskEL Project "Synchronous Condenser Application in Low Inertia Power Systems (SCAPP)" under Grant 12196, administrated by Energinet.

Jundi Jia, Guangya Yang and Arne Hejde Nielsen are with the Center for Electric Power and Energy, Department of Electrical Engineering, Technical University of Denmark, Kgs. Lyngby, Denmark (e-mail: junjia@elektro.dtu.dk; gyy@elektro.dtu.dk; ahn@elektro.dtu.dk).

Peter Rønne-Hansen is with Siemens A/S, Ballerup, Denmark (e-mail: peter.r.hansen@siemens.com).

With conventional power plants gradually replaced by converter-based generations, a future power system may experience significant drops on the system short circuit strength. This could raise problems such as voltage instability, undesirable dynamic behaviors of converters and malfunctions of protection systems. Since the short circuit response of a synchronous condenser (SC) resembles that of a synchronous generator, SCs may serve as an alternative to improve the system short circuit strength and thus the application of SCs has gained increasing attention in recent years [25]–[29]. The refurbishment of conventional power plants to SCs have been proposed in [27], [28] to address dynamic voltage control issues and improve system short circuit ratios. However, conventional power plants may not always serve as the best locations for SCs and newly-installed SCs can be anticipated. The studies in [28], [29] have presented methods on the optimal allocation of SCs minimizing the total cost. The results have suggested that there is a need of installing new SCs for more VSCs. Therefore, it is necessary to examine the cooperation of VSC and SC from protection perspective considering different VSC control strategies, which has not been investigated in the previous studies.

This paper investigates the impact of different VSC control strategies and the impact of incorporating synchronous condensers on distance protection under unbalanced faults through HIL tests. Three representative control strategies from the literature, namely constant active power, balanced current and constant reactive power control, are examined systematically. In order to limit the converter current in each phase, a generic converter peak current limitation method is derived for the examined control strategies. The tests are designed based on the variations of the sources of short circuit current, VSC control strategies, SC capacities, fault locations and types. According to the tests results from the commercial relay, we propose to avoid using constant reactive power control strategy, while constant active power and balanced current control strategies favor the performances of distance protection.

The rest of this paper is organized as follows. Section II outlines VSC control strategies under unbalanced faults. A generic converter peak current limitation method is derived for the examined control strategies. Synchronous condensers are shortly introduced in Section III. Section IV presents a systematic HIL evaluation on the impact of different VSC control strategies and incorporation of synchronous condensers on distance protection. In Section V, HIL tests are conducted on the western Danish power system for further verifications. Finally, conclusions are provided in Section VI.

II. Voltage Source Converter Control

A. Control Strategies

Typically, the control system of a grid-connected VSC system consists of a slower outer controller and a faster inner current controller. The inner current controller is responsible to track the current references generated by the outer controller. For a three-phase three-wire VSC, zero-sequence components are not present. Therefore, the instantaneous active and reactive powers at the PCC can be expressed by (1) and (2) using the instantaneous power theory [30]:

$$p = \underbrace{\overbrace{\mathbf{v}^+ \cdot \mathbf{i}_P^+}^{P^+} + \overbrace{\mathbf{v}^- \cdot \mathbf{i}_P^-}^{P^-}}_{\overline{P}} + \underbrace{\mathbf{v}^+ \cdot \mathbf{i}_P^- + \mathbf{v}^- \cdot \mathbf{i}_P^+}_{\widetilde{P}} \tag{1}$$

$$q = \underbrace{\overbrace{\mathbf{v}_\perp^+ \cdot \mathbf{i}_Q^+}^{Q^+} + \overbrace{\mathbf{v}_\perp^- \cdot \mathbf{i}_Q^-}^{Q^-}}_{\overline{Q}} + \underbrace{\mathbf{v}_\perp^+ \cdot \mathbf{i}_Q^- + \mathbf{v}_\perp^- \cdot \mathbf{i}_Q^+}_{\widetilde{Q}} \tag{2}$$

where $\mathbf{v} = [v_a \;\; v_b \;\; v_c]^T$ and $\mathbf{i} = [i_a \;\; i_b \;\; i_c]^T$ represent the instantaneous voltage and current vectors at the PCC; the operator "·" denotes the arithmetic dot product of vectors; the superscripts "+" and "−" represent the positive- and negative-sequence components; the subscript "⊥" refers to an orthogonal version of the original vector (e.g., $\mathbf{v}^+$ leads $\mathbf{v}_\perp^+$ by 90° with the same amplitude; $\mathbf{v}^-$ leads $\mathbf{v}_\perp^-$ by 90° with the same amplitude); $\overline{P}$ and $\overline{Q}$ are constant power terms resulting from the interaction between the voltage and current in the same sequence. They consist of positive-sequence power terms (P^+, Q^+) and negative-sequence power terms (P^-, Q^-). $\widetilde{P}$ and $\widetilde{Q}$ are oscillating power terms due to the interaction between the voltage and current in different sequences. With (1) and (2), the current references can be constructed in different ways, giving the short circuit current from a VSC diverse characteristics.

In [8], a flexible control over the relative amplitudes of oscillating active and reactive powers is presented. Two adjustable scalars k_p and k_q are introduced in current references:

$$\mathbf{i}_P^{ref} = \frac{P^{ref}}{|\mathbf{v}^+|^2 + k_p |\mathbf{v}^-|^2}(\mathbf{v}^+ + k_p \mathbf{v}^-) \tag{3}$$

$$\mathbf{i}_Q^{ref} = \frac{Q^{ref}}{|\mathbf{v}^+|^2 + k_q |\mathbf{v}^-|^2}(\mathbf{v}_\perp^+ + k_q \mathbf{v}_\perp^-) \tag{4}$$

where P^{ref} and Q^{ref} are active and reactive power references; $\mathbf{i}_P^{ref}$ and $\mathbf{i}_Q^{ref}$ are active and reactive current references respectively. With (3) and (4) substituted into (1) and (2), the oscillating power terms can be expressed as:

$$\widetilde{P} = \frac{(1+k_p)P^{ref}}{D_p}\mathbf{v}^+\mathbf{v}^- + \frac{(1-k_q)Q^{ref}}{D_q}\mathbf{v}_\perp^+\mathbf{v}^- \tag{5}$$

$$\widetilde{Q} = \frac{(1+k_q)Q^{ref}}{D_q}\mathbf{v}_\perp^+\mathbf{v}_\perp^- + \frac{(1-k_p)P^{ref}}{D_p}\mathbf{v}^+\mathbf{v}_\perp^- \tag{6}$$

$$D_p = |\mathbf{v}^+|^2 + k_p |\mathbf{v}^-|^2, \;\; D_q = |\mathbf{v}^+|^2 + k_q |\mathbf{v}^-|^2 \tag{7}$$

In this paper, three most representative scenarios are considered: 1) *Constant active power control*: the oscillations in active power are nullified with $k_p = -1$ and $k_q = 1$; the short circuit current contains negative-sequence component; 2) *Balanced current control*: the short circuit current contains only positive-sequence component with $k_p = k_q = 0$. Oscillations with the same amplitude are registered in active and reactive powers; 3) *Constant reactive power control*: oscillation-free reactive power is achieved with $k_p = 1$ and $k_q = -1$; the short circuit current contains negative-sequence component.

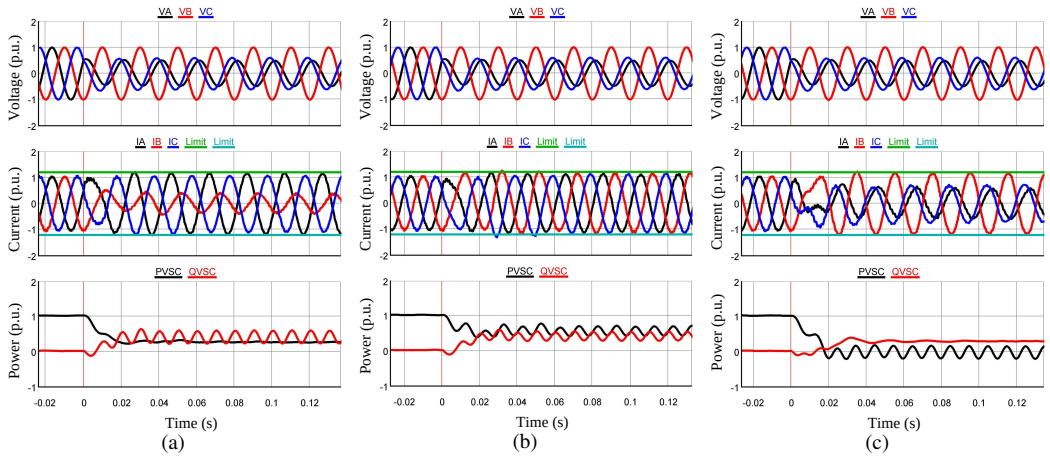

Fig. 1. Short circuit response of a VSC (with 1.2 p.u. converter current limit) to an A–g fault on wye-winding side: (a) Constant active power control. (b) Balanced current control. (c) Constant reactive power control. (Measurements are taken from the delta-winding side.)

B. Converter Current Limit

When the PCC experiences a voltage dip, the current references can become dangerously high if the active and reactive power references remain unchanged. This may damage power electronic devices and result in an undesirable disconnection of the converter from the grid. Therefore, the active and reactive power references should be reduced properly to safely guard the current within its limit in each individual phase.

In [14], a peak current limitation method is presented by fully utilizing the power capacity of the converter. It is capable of injecting active and reactive powers simultaneously with the current in each phase restricted. However, the derived equations cannot be directly used if current references are chosen as (3) and (4). According to the current ellipse theory presented in [9], the relationship among the values of phase-A peak current $\hat{I}$, average active power and average reactive power can be expressed by (8)–(11):

$$\hat{I}^2 = (I_{pL}\cos\gamma - I_{qL}\sin\gamma)^2 + (I_{qS}\cos\gamma + I_{pS}\sin\gamma)^2 \quad (8)$$

$$I_{pL} = \frac{P^+}{|\mathbf{v}^+|} + \frac{P^-}{|\mathbf{v}^-|},\quad I_{pS} = \frac{P^+}{|\mathbf{v}^+|} - \frac{P^-}{|\mathbf{v}^-|} \quad (9)$$

$$I_{qL} = \frac{Q^+}{|\mathbf{v}_\perp^+|} + \frac{Q^-}{|\mathbf{v}_\perp^-|},\quad I_{qS} = \frac{Q^+}{|\mathbf{v}_\perp^+|} - \frac{Q^-}{|\mathbf{v}_\perp^-|} \quad (10)$$

$$\gamma = \frac{|\phi^+| - |\phi^-|}{2} \quad (11)$$

where I_{pL} and I_{pS} are the values of the long and short axes of the active current ellipse; I_{qL} and I_{qS} are that of the reactive current ellipse; ϕ^+ and ϕ^- are the phase angles of positive- and negative-sequence voltages respectively. With (3) and (4) taken as current references, (9) and (10) can be rewritten as:

$$I_{pL} = P\frac{(|\mathbf{v}^+| + k_p|\mathbf{v}^-|)}{|\mathbf{v}^+|^2 + k_p|\mathbf{v}^-|^2}, I_{pS} = P\frac{(|\mathbf{v}^+| - k_p|\mathbf{v}^-|)}{|\mathbf{v}^+|^2 + k_p|\mathbf{v}^-|^2} \quad (12)$$

$$I_{qL} = Q\frac{(|\mathbf{v}^+| + k_q|\mathbf{v}^-|)}{|\mathbf{v}^+|^2 + k_q|\mathbf{v}^-|^2}, I_{qS} = Q\frac{(|\mathbf{v}^+| - k_q|\mathbf{v}^-|)}{|\mathbf{v}^+|^2 + k_q|\mathbf{v}^-|^2} \quad (13)$$

By substituting (11)–(13) into (8), a quadratic equation can be derived if P is considered as an unknown variable. The solution of this quadratic equation can be obtained by:

$$P = \frac{-B + \sqrt{(B^2 - 4AC)}}{2A} \quad (14)$$

$$A = y^2\left(m^2\cos^2\gamma + n^2\sin^2\gamma\right) \quad (15)$$

$$B = -2Qxy\sin\gamma\cos\gamma(mr - ns) \quad (16)$$

$$C = Q^2x^2\left(r^2\sin^2\gamma + s^2\cos^2\gamma\right) - x^2y^2\hat{I}^2 \quad (17)$$

$$m = |\mathbf{v}^+| + k_p|\mathbf{v}^-|,\ n = |\mathbf{v}^+| - k_p|\mathbf{v}^-| \quad (18)$$

$$r = |\mathbf{v}^+| + k_q|\mathbf{v}^-|,\ s = |\mathbf{v}^+| - k_q|\mathbf{v}^-| \quad (19)$$

$$x = |\mathbf{v}^+|^2 + k_p|\mathbf{v}^-|^2,\ y = |\mathbf{v}^+|^2 + k_q|\mathbf{v}^-|^2 \quad (20)$$

As long as the values of Q and $\hat{I}$ are given, the maximum active power P_a that is permitted without exceeding current limit in phase-A can be determined. With the value of γ changed to $(|\phi^+| - |\phi^-|)/2 + \pi/3$ and $(|\phi^+| - |\phi^-|)/2 - \pi/3$ respectively, the maximum active power P_b and P_c can also be derived for phase-B and phase-C [9] by using (14)–(20). Therefore, the maximum permitted active power P^{limit} can be decided by:

$$P^{limit} = \min\{P_a, P_b, P_c\} \quad (21)$$

However, the equations above assume that the current limit is not reached by only injecting reactive power. In order to impose a limit on reactive power, a similar procedure of deriving P^{limit} is performed, where Q is regarded as an unknown variable instead of P and the value of P is set to zero. Then the limit for reactive power can be expressed by:

$$Q^{limit} = \min\{Q_a, Q_b, Q_c\} \quad (22)$$

In order to illustrate the effectiveness of the above equations, the presented method with $\hat{I} = 1.2$ p.u. is implemented in the control system of a VSC. The VSC is connected to the delta winding of the interface transformer. The wye winding, whose neutral is solidly grounded, is connected to the grid. With an A–g fault applied at wye-winding side of the transformer, the corresponding three-phase voltage, three-phase current and output powers measured at delta-winding side are given in Fig. 1 as an example, where reactive power injection is prioritized. As expected, the fault current supplied by the converter is restricted within 1.2 p.u. in each phase after initial transients.

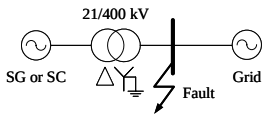

Fig. 2. Single-line diagram of the system for showing SG and SC response.

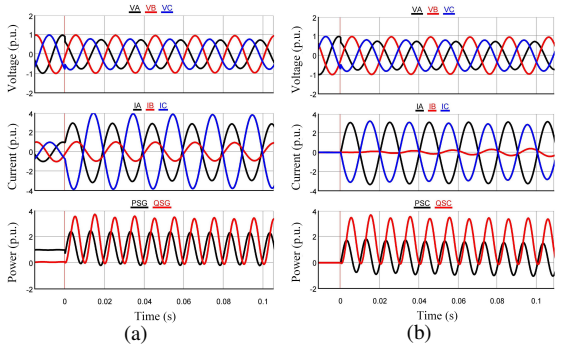

Fig. 3. Short circuit response of synchronous sources to an A–g fault on wye-winding side: (a) Synchronous generator. (b) Synchronous condenser. (Measurements are taken from the delta-winding side)

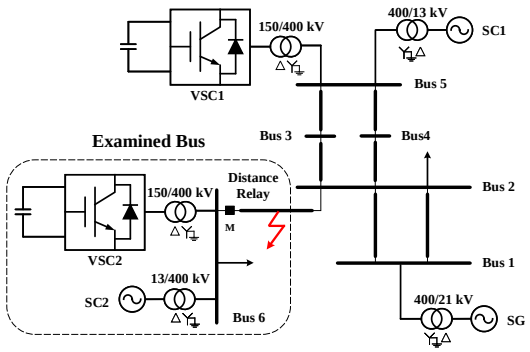

Fig. 4. Single-line diagram of the 400 kV test system

III. SC Responses under Unbalanced Faults

A synchronous condenser (SC) is a synchronous machine without a prime mover. During the start-up phase, the rotor of the SC can be driven to the synchronous speed by a speed-controlled motor [31]. Once the synchronous speed is reached, the field is supplied and then the SC can be connected to the grid. Since there is no mechanical torque provided to its shaft, SC cannot provide sustaining active power. Depending on the excitation level performed by the automatic voltage regulator, an SC can either generate or absorb reactive power in the steady state. One benefit of applying SC is that it can help to increase the system short circuit strength. It can provide short circuit current with a similar magnitude as a synchronous generator (SG) does to dynamically support the grid voltage. In order to illustrate the effect clearly, a simple system shown in Fig. 2 is simulated with SG or SC as an example. Both SG and SC share the same parameters. In steady state, they are controlled to exchange zero reactive power with the grid and SG deliveries 1 p.u. active power. Figure 3 compares their response to an A–g fault on the high voltage side.

As shown in Fig. 3, both SG and SC provide a considerable amount of reactive power to the grid during the fault. Since SC is a rotating machine, it also provides inertia for the system resulting in its active power exchange with the grid during the transients. This is another benefit of using SC. By comparing Fig. 3 to Fig. 1, it can be observed that the short circuit current from synchronous sources in phase-A and phase-C is more than three times higher than that of the VSC. In Fig. 3, the currents in phase-A and phase-C are almost out of phase by 180°. However, the current phases in Fig. 1 are mainly affected by the VSC control strategy. Among the three examined control strategies, constant active power control yields short circuit current most similar to that of Fig. 3 in terms of phases. The short circuit current in balanced current control is completely symmetrical. For constant reactive power control, the currents in phase-A and phase-C are closer to be in phase rather than out of phase. Therefore, there might exist certain impacts on distance protection under unbalanced faults when replacing SG with VSC and applying an SC at the PCC.

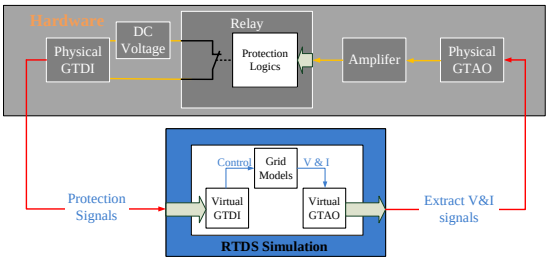

Fig. 5. Hardware-in-the-loop test platform.

TABLE I
TEST SYSTEM PARAMETERS

VSC1 Rating	500 MW	Line 1–2	$15\angle 87^\circ\,\Omega$
VSC2 Rating	500 MW	Line 2–3 & 2–4	$14\angle 87^\circ\,\Omega$
SG Rating	600 MW	Line 3–5 & 4–5	$18\angle 86^\circ\,\Omega$
SC1 Rating	160 Mvar	Line 6–2	$9\angle 86^\circ\,\Omega$
SC2 Rating	50–250 Mvar	VT	400 kV/100 V
VSC DC voltage	350 kV	CT	1000 A/1 A

IV. Case Studies

A. System Overview

The investigation is firstly tested on a 400 kV system shown in Fig. 4. A synchronous generator (SG) is connected to bus 1 (slack bus). Two VSCs (VSC1 and VSC2) are connected to bus 5 and 6 respectively. Balanced current control is deployed for VSC1 while the control strategy of VSC2 can be freely shifted among constant active power, balanced current and constant reactive power control. Under fault conditions, reactive power injection takes the first priority and its reference is calculated using $Q_{ref} = |\mathbf{v}^+| \cdot I_Q$. The value of I_Q is obtained from [32] and it can be expressed as $I_Q = -2.5\,|\mathbf{v}^+| + 2.25$ $(0 \leq I_Q \leq 1)$. To enhance the fault-ride-through operation of the VSCs, both VSCs are equipped with a dynamic braking resistor on the DC side to drain the excess electrostatic energy according to [33]. Synchronous condensers SC1 and SC2 are equipped at the PCC of these two converters. The capacity of SC2 can be varied from 50 Mvar to 250 Mvar with a 50 Mvar step. A distance relay is used to protect line 6–2 at the terminal near bus 6. Further details of the system are listed in Table I. In steady state, VSC1 and VSC2 deliver 325 MW and 500 MW active power respectively with unity power factor while SG delivers 175 MW active power.

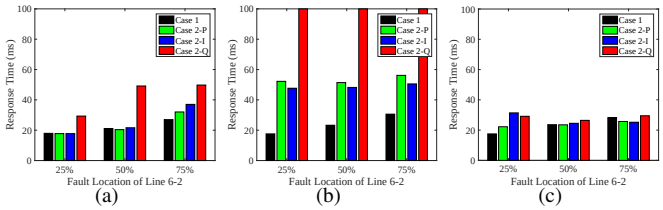

Fig. 6. Average response time for Case 1 and Case 2: (a) A–g fault. (b) A–B fault. (c) A–B–g fault. (100 ms in (b) represents refuse-to-trip failure)

In this paper, the investigation is conducted through HIL tests using a commercial distance relay in real time. As illustrated in Fig. 5, the grid models are simulated in Real Time Digital Simulator (RTDS). The three-phase voltage and current signals needed by the distance relay are firstly extracted from simulations using a Gigabit Transceiver Analogue Output Card (GTAO). Since the maximum output voltage of its terminal is limited by +/-10 V, the signals measured from the secondary sides of the CT and VT in simulations have to be scaled down properly by adjusting the output scaling factor of the virtual GTAO component in RTDS. Then, an amplifier scales up the signals measured from the GTAO so that amplified signals equal to the real values obtained from the CT and VT. The protection signal generated by the relay is sent back to RTDS using a Gigabit Transceiver Digital Input Card (GTDI). When there is no current through its terminal, the digital input read by the RTDS processor card will be a logic "0". In order to change the value to logic "1", an external 5 V signal is needed to drive the current into the GTDI terminal. Since the distance relay uses a potential-free switch, a 5 V DC voltage source is connected in series with the switch and GTDI terminals. Therefore, a logic "1" will be registered if the switch closes, forming a closed loop for the HIL test setup. In the following case studies, the zone-1 performances of the relay using the classic method are evaluated. This study does not involve relay coordination and communication. The relay is set to protect 90% of line 6–2 with the quadrilateral characteristic. Solid A–g, A–B, and A–B–g faults are simulated at 25%, 50% and 75% of line 6–2 respectively. The zero time instant corresponds to the instant when the fault is initiated. The response time of each test is defined as the time elapsed from the fault being initiated until the protection signal being registered in RTDS.

B. Case 1: Synchronous generator solely

In this case, a more traditional power system is simulated by replacing VSC2 with a 500 MVA synchronous generator and disconnecting SC2. Therefore, the short circuit current seen by the distance relay is only contributed by the synchronous generator. For each fault type and location, the HIL tests are repeated 10 times. All the faults are initiated when the phase-A voltage of bus 6 crosses zero from the negative to the positive in order to ensure each test has the same pre-fault conditions.

C. Case 2: Voltage source converter solely

This case tests the system in Fig. 4 with SC2 disconnected so that the short circuit current seen by the relay is solely

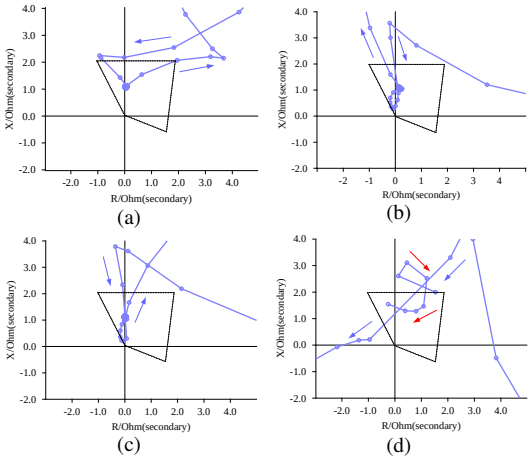

Fig. 7. Impedance plane of AB element for A–B fault at 50% of line 6–2: (a) Case1. (b) Case2–P. (c) Case2–I. (d) Case2–Q.

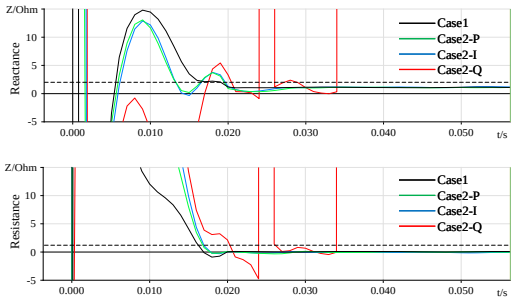

Fig. 8. Measured impedance values for A–B fault at 50% of line 6–2.

provided by VSC2. The control strategy of VSC2 under unbalanced faults are shifted among constant active power (Case2–P), balanced current (Case2–I) and constant reactive power (Case2–Q) control. The converter current limit is set to 1 p.u. in each phase for both VSC1 and VSC2. For each type and location of the faults specified above, the tests are repeated 10 times as Case 1.

The average response time for Case 1 and Case 2 is summarized in Fig. 6 for different fault types and locations. Compared with Case 1, the response time in Case 2 generally increases, especially for A–B faults. This indicates that the sensitivity of distance protection might be deteriorated as a result of low short circuit current level in converter-dominated power systems. Among the three examined control strategies, constant active power and balanced current control give similar performances in terms of response time. However, with constant reactive power control used for VSC2, the sensitivity of the relay is impacted significantly for A–g faults and the relay even fails to trip under A–B faults. As an example, Fig. 7 presents the impedance plane given by the relay when an A–B fault occurs at 50% of line 6–2 for Case 1 and 2. By comparing Fig. 7(b)–(c) to Fig. 7(a), more transients are observed before the locus stabilizes at the indicated fault location inside the zone. However, in Fig. 7(d), the impedance locus exhibits unfavorable characteristics. Even though the locus enters zone-1, it does not indicate a fault location clearly. Corresponding to each scenario in Fig. 7, the measured impedance versus time is further plotted in Fig. 8. The curve for Case2-Q moves in

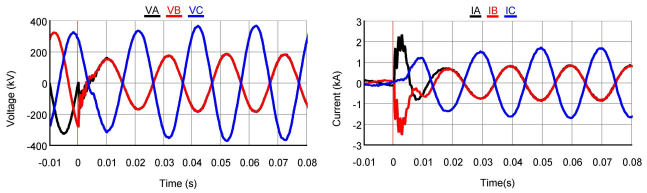

Fig. 9. Inputs (primary-side values) to distance relay for A–B fault at 50% of line 6–2. (Case2-Q)

and out from the effective zone during the fault while the curves for the other three scenarios stay inside the effective zone stably during the fault.

Corresponding to Case2-Q in Fig. 7(d), Fig. 9 presents the three-phase voltage and current inputs to the relay. The three-phase voltage (from the wye-winding side of the converter transformer) under fault conditions can be approximately represented by $\mathbf{v}_y$. If it is referred to the delta-winding side, the voltage becomes $\mathbf{v}_\Delta$:

$$\mathbf{v}_y = \begin{bmatrix} M_1 sin(\omega t) \\ M_1 sin(\omega t) \\ -M_2 sin(\omega t) \end{bmatrix}, \ \mathbf{v}_\Delta = \begin{bmatrix} M_3 sin(\omega t) \\ 0 \\ -M_3 sin(\omega t) \end{bmatrix} \tag{23}$$

where M_1, M_2 and $M_3 = (M_1 + M_2)/(\sqrt{3}N)$ represent the magnitudes of the corresponding voltages. N refers to the turns ratio of the transformer from the wye-winding side to the delta-winding side. By decomposing $\mathbf{v}_\Delta$ into its symmetrical components, there are:

$$\begin{bmatrix} v_a^+ \\ v_b^+ \\ v_c^+ \end{bmatrix} = \begin{bmatrix} M_4 sin(\omega t + \frac{\pi}{6}) \\ M_4 sin(\omega t - \frac{\pi}{6}) \\ M_4 sin(\omega t + \frac{5\pi}{6}) \end{bmatrix}, \ \begin{bmatrix} v_a^- \\ v_b^- \\ v_c^- \end{bmatrix} = \begin{bmatrix} M_4 sin(\omega t - \frac{\pi}{6}) \\ M_4 sin(\omega t + \frac{\pi}{6}) \\ M_4 sin(\omega t - \frac{5\pi}{6}) \end{bmatrix} \tag{24}$$

where $M_4 = (M_1 + M_2)/(3N)$ represents the magnitudes of the corresponding voltages. Then, the orthogonal versions of the positive- and negative-sequence voltages are given by:

$$\begin{bmatrix} v_{a\perp}^+ \\ v_{b\perp}^+ \\ v_{c\perp}^+ \end{bmatrix} = \begin{bmatrix} M_4 sin(\omega t - \frac{\pi}{3}) \\ M_4 sin(\omega t - \pi) \\ M_4 sin(\omega t + \frac{\pi}{3}) \end{bmatrix}, \ \begin{bmatrix} v_{a\perp}^- \\ v_{b\perp}^- \\ v_{c\perp}^- \end{bmatrix} = \begin{bmatrix} M_4 sin(\omega t + \frac{\pi}{3}) \\ M_4 sin(\omega t + \pi) \\ M_4 sin(\omega t - \frac{\pi}{3}) \end{bmatrix} \tag{25}$$

With current references (3) and (4) deployed, the phases of $\mathbf{i}_P^{ref}$ and $\mathbf{i}_Q^{ref}$ are solely decided by the phases of the voltages ($\mathbf{v}^+$, $\mathbf{v}^-$, $\mathbf{v}_\perp^+$ and $\mathbf{v}_\perp^-$) and the values of the flexible scalars (k_p and k_q). Therefore, by substituting (24) and (25) into (3) and (4), the current references expressed in abc-frame for constant active power control strategy can be represented by:

$$\mathbf{i}_P^{ref} = \frac{P^{ref}}{|\mathbf{v}^+|^2 - |\mathbf{v}^-|^2} \begin{bmatrix} v_a^+ - v_a^- \\ v_b^+ - v_b^- \\ v_c^+ - v_c^- \end{bmatrix} = M_5 \begin{bmatrix} cos(\omega t) \\ -2cos(\omega t) \\ cos(\omega t) \end{bmatrix} \tag{26}$$

$$\mathbf{i}_Q^{ref} = \frac{Q^{ref}}{|\mathbf{v}^+|^2 + |\mathbf{v}^-|^2} \begin{bmatrix} v_a^+ + v_a^- \\ v_b^+ + v_b^- \\ v_c^+ + v_c^- \end{bmatrix} = M_6 \begin{bmatrix} sin(\omega t) \\ -2sin(\omega t) \\ sin(\omega t) \end{bmatrix} \tag{27}$$

while for constant reactive power control strategy, there are:

$$\mathbf{i}_P^{ref} = \frac{P^{ref}}{|\mathbf{v}^+|^2 + |\mathbf{v}^-|^2} \begin{bmatrix} v_{a\perp}^+ + v_{a\perp}^- \\ v_{b\perp}^+ + v_{b\perp}^- \\ v_{c\perp}^+ + v_{c\perp}^- \end{bmatrix} = M_7 \begin{bmatrix} sin(\omega t) \\ 0 \\ -sin(\omega t) \end{bmatrix} \tag{28}$$

$$\mathbf{i}_Q^{ref} = \frac{Q^{ref}}{|\mathbf{v}^+|^2 - |\mathbf{v}^-|^2} \begin{bmatrix} v_{a\perp}^+ - v_{a\perp}^- \\ v_{b\perp}^+ - v_{b\perp}^- \\ v_{c\perp}^+ - v_{c\perp}^- \end{bmatrix} = M_8 \begin{bmatrix} cos(\omega t) \\ 0 \\ -cos(\omega t) \end{bmatrix} \tag{29}$$

where M_5-M_8 represent the magnitudes of the currents. As the currents are restricted in magnitudes and the phase information is of interest here, M_5-M_8 are not given explicitly for brevity. If the currents expressed by (26)-(29) are referred back to the wye-winding side, the current in phase-A and phase-B will be out of phase (similiar to that of synchronous generators during A–B faults) with (26) and (27). However, for constant reactive power control with (28) and (29), the current in phase-A and phase-B will be in phase with the same magnitude, which is significantly different from that of a synchronous source. Typically, the apparent impedance given by the AB element of a distance relay is calculated by [34]:

$$Z_{AB} = \frac{\dot{V}_A - \dot{V}_B}{\dot{I}_A - \dot{I}_B} \tag{30}$$

where $\dot{V}_A$, $\dot{V}_B$ and $\dot{I}_A$, $\dot{I}_B$ are the voltage and current inputs expressed in phasors. Therefore, currents being identical in phase and amplitude (Fig. 9) may give a zero value in the denominator of (30). This makes the distance relay unable to calculate the impedance reliably, which explains why discontinuous locus and curves are present for Case2-Q with constant reactive power control strategy. Such discontinuous features in AB elements can also be observed under A–B–g faults with constant reactive power control. Since the operation of distance relay under A–B–g faults also relies on AG and BG elements, the relay can operate successfully. However, the use of constant reactive power control still adversely impacts the reliability of the distance relay.

D. Case 3: Incorporation of synchronous condensers

In order to evaluate the combined effect of VSC and SC on the distance relay when an SC is equipped at the PCC of a VSC, the system in Fig. 4 is simulated with SC2 connected. Therefore, the fault current seen by the relay is jointly provided by VSC2 and SC2. In addition, the capacity of SC2 is varied among 50, 100, 150, 200 and 250 Mvar as different scenarios. To ensure Case 2 and Case 3 has the same pre-fault conditions, the excitation of SC2 is adjusted in each scenario so that Case 3 has the same power flow results as Case 2 prior to the fault. The same HIL tests are repeated under different VSC2 control strategies and SC2 capacities.

Firstly, the DC-link voltages of VSC2 under different scenarios are shown in Fig. 10. With the dynamic braking resistor, the DC-link voltages are restricted within 1.1 p.u. of the nominal value. According to Fig. 10(a), constant active power control gives nearly zero oscillation in the DC-link voltage,

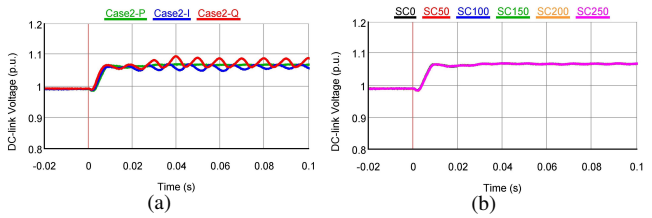

Fig. 10. Comparison on the VSC2 DC-link voltages for A–B fault at 50% of line 6–2: (a) Case 2. (b) Case 3 with constant active power control in VSC2. (The number in the legend represents the capacity of SC2)

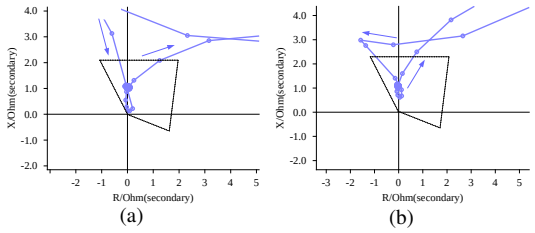

Fig. 11. Impedance plane of AB element for A–B fault at 50% of line 6–2 in Case 3 with constant reactive power control: (a) SC2: 100 Mvar. (b) SC2: 200 Mvar.

while constant reactive power control yields the largest oscillations. On the other hand, as shown in Fig. 10(b), different SC2 capacities have almost no notable effect on the DC-link voltages if the control strategy of VSC2 is fixed.

With the help of SC2, the measured impedance locus is generally improved with fewer transients in Case 3. As an illustration, with constant reactive power control deployed, Fig. 11 presents the impedance plane under A–B faults at 50% of line 6–2 when a 100 Mvar or a 200 Mvar SC2 is applied. In contrast to Fig. 7(d), the locus in Fig. 11 stabilizes at the indicated fault location inside the zone and moves out of the zone after the fault is cleared by the relay. The average response time in Case 3 is summarized in Fig. 12 with different SC2 capacities, where the results from Case 1 (black dashed line) and Case 2 (points corresponding to 0 Mvar) are also included for the sake of comparison.

With the capacity of SC2 increased from 0 to 250 Mvar, the speed of the distance relay is improved generally and getting closer to that of Case 1. However, with a 50 Mvar SC2, the relay still fails to operate when constant reactive power control is deployed. On the one hand, the capacity of a 50 Mvar SC2 is relatively small compared to a 500 MVA VSC2 and hence the short circuit current from SC2 is not significant in terms of amplitudes compared with that from VSC2. On the other hand, as discussed above, the phases of the short circuit current from VSC2 under unbalanced faults can differ from that of SC2 significantly. As shown in Fig. 1–2 and derived in (23)-(29), constant active power control yields the most similar short circuit current to that of synchronous sources, while constant reactive power control gives the largest deviation in terms of phases. Therefore, due to the differences in the current phases, the application of SC2 at the PCC may even further reduce the short circuit current level when constant reactive power control is used. In order to illustrate this problem, Fig. 13 compares the combined short circuit currents of VSC2 and SC2 in phase-A for an A–B fault at 50% of line 6–2 with different capacities

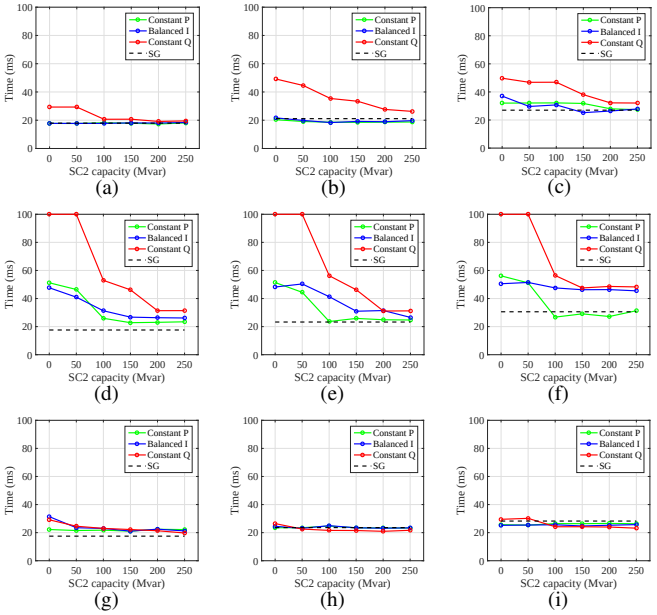

Fig. 12. Average response time for Case 1, 2 and 3: (a) A–g fault at 25%. (b) A–g fault at 50%. (c) A–g fault at 75%. (d) A–B fault at 25%. (e) A–B fault at 50%. (f) A–B fault at 75%. (g) A–B–g fault at 25%. (h) A–B–g fault at 50%. (i) A–B–g fault at 75%. (100 ms in (d)–(f) represents refuse-to-trip failure)

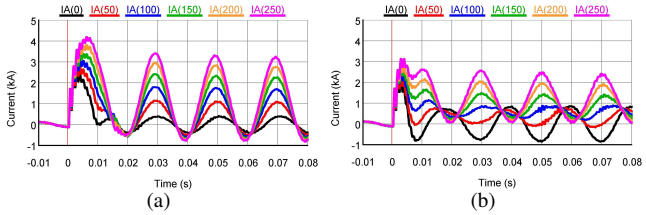

Fig. 13. Comparison on the fault current in phase-A with different SC2 capacity for A–B fault at 50% of line 6–2: (a) Constant active power control. (b) Constant reactive power control. (The number in the legend represents the capacity of SC2)

of SC2. For constant active power control in Fig. 13(a), the amplitude of the current is gradually boosted by increasing SC2 capacity. However, for constant reactive power control in Fig. 13(b), compared to the scenario without SC2 (IA(0)), the amplitude of the current is even reduced when a 50 Mvar SC2 is used (IA(50)). This effect makes the combined short circuit current such small that it is even not enough to activate the distance relay for impedance calculation. Even though the relay can operate successfully by further increasing the capacity of SC2, the total available short circuit current in Fig. 13(b) is less than that in Fig. 13(a) with a SC2 of the same capacity. This suggests that constant reactive power control impairs the advantages of synchronous condensers due to the phase differences between the short circuit current from the VSC and the SC.

As shown in Fig. 6(a) and Fig. 6(c), the relay performances under grounded faults are not impacted so much if constant active power or balanced current control is used. Since the wye-winding side of VSC2 interface transformer is solidly grounded, it provides a path for the zero-sequence current to flow under grounded faults. As a result, the current limita-

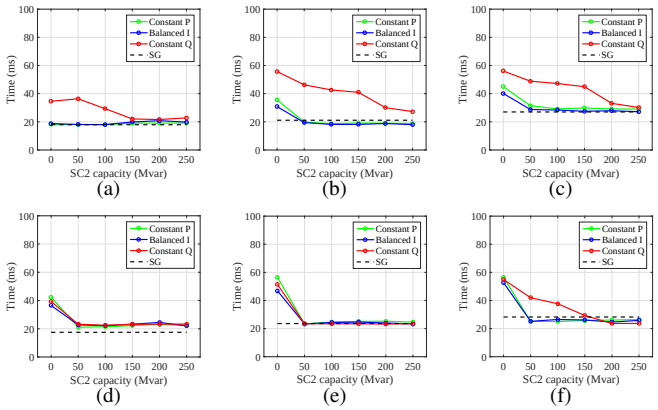

Fig. 14. Average response time for Case 4: (a) A–g fault at 25%. (b) A–g fault at 50%. (c) A–g fault at 75%. (d) A–B–g fault at 25%. (e) A–B–g fault at 50%. (f) A–B–g fault at 75%.

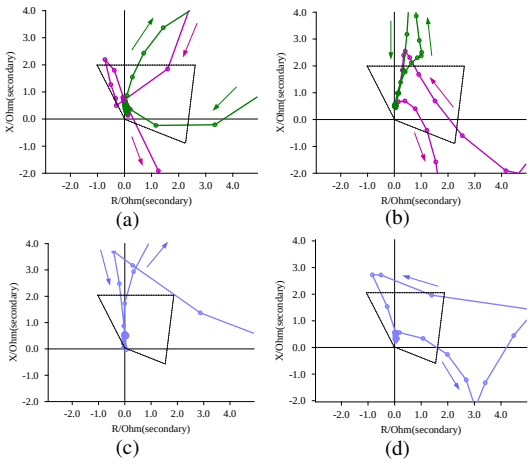

Fig. 15. Impedance plane for A–B–g fault at 25% of line 6–2 in Case 4 with balanced current control: (a) AG and BG elements, no SC2. (b) AG and BG elements, with 50 Mvar SC2. (c) AB element, no SC2. (d) AB element, with 50 Mvar SC2.

tion of VSC has less impact on the relay performances for grounded faults if zero-sequence current with high amplitudes is present. In order to investigate the relay performances when there is a lack of zero-sequence current, a 300 Ω grounding resistance is added to the grounding branch of the VSC2 interface transformer. The same tests in Case 2 and Case 3 are repeated for A–g and A–B–g faults. The average response time of the relay is summarized in Fig. 14, which is denoted as Case 4. By comparing Fig. 14(a)–(c) to Fig. 12(a)–(c) or comparing Fig. 14(d)–(f) to Fig. 12(g)–(i), the response time increases in Case 4 when there is no SC2 connected (0 Mvar). Once SC2 is connected to the system, the response time is brought back for constant active and balanced current control. This is because the step-up transformer of SC2 provides a path for the zero-sequence current that helps the relay operation. However, constant reactive power control still yields the worst performances because its use reduces the combined short circuit current from VSC and the rest of the system. Figure 15 presents the impedance plane of AG, BG and AB elements for an A–B–g fault at 25% of line 6–2 when there is no SC2 (Fig. 15(a) and (c)) and when there is a 50 Mvar SC2 connected

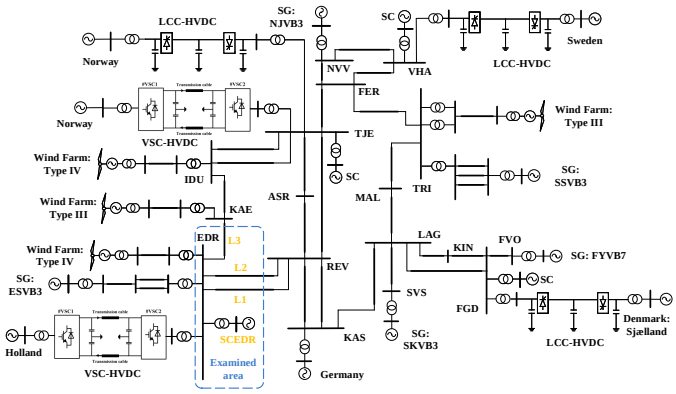

Fig. 16. Single-line diagram of a simplified western Danish power system

TABLE II
DIFFERENT TOPOLOGIES OF THE EXAMINED AREA PRIOR TO FAULTS

	Component			
Topology	L1	L2	L3	SCEDR
T1	Y	N	N	N
T2	Y	N	N	Y
T3	Y	N	Y	N
T4	Y	N	Y	Y
T5	Y	Y	Y	N

(Fig. 15(b) and (d)). By comparing Fig. 15(a) to Fig. 15(b), it can be observed that the locus exhibits more transients when zero-sequence current is limited.

According to the test results in Fig. 12 and Fig. 14, the improvement in the relay speed correlates with the VSC2 control strategy and the SC2 capacity. For the test system in this paper, a SC2 of 100 Mvar at bus 6 is a good choice for constant active power control since the improvement in speed starts to saturate with higher SC2 capacities. Similarly, a SC2 of 150 Mvar is an optimal choice for balanced current control. Besides requiring a higher capacity of SC2, balanced current control does not perform as well as constant active power control for phase-phase faults (Fig. 12(e)–(f)). In the worst case, constant reactive power control requires a synchronous condenser of at least 200 Mvar to achieve similar performances as the other two control strategies.

V. TESTS ON WESTERN DANISH POWER SYSTEM

In this section, the HIL tests are further conducted on a larger power system with more integrated converters. Figure 16 presents the single-line diagram of the simplified western Danish power system (DK1), where each 400 kV bus is assigned a three-letter name. The system is developed based on the present DK1 in [28], [35], but with new planed lines to represent a future scenario. In order to generate a future case, three conventional SGs (ESVB3, NJVB3 and SKVB3) are assumed to be phased out and disconnected from the system. In the following studies, the tests are performed regarding the distance relay located on L1 near bus EDR. The relay is set to protect 90% of L1. Five different topologies of the examined area are considered, which are summarized in Table II. For example, topology 2 (T2) means L1 and SCEDR are present while L2 and L3 are disconnected from the system. Prior to a fault on L1, all five HVDC links and three wind

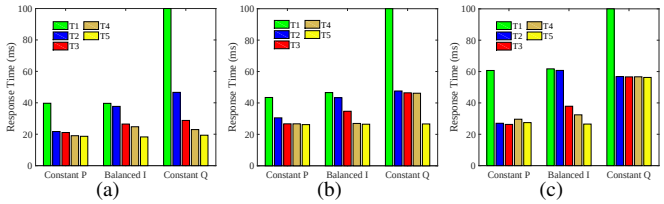

Fig. 17. Average response time of the distance relay under different pre-fault topologies for an A–B fault at: (a) 25% of L1. (b) 50% of L1. (c) 75% of L1. (100 ms represents refuse-to-trip failure)

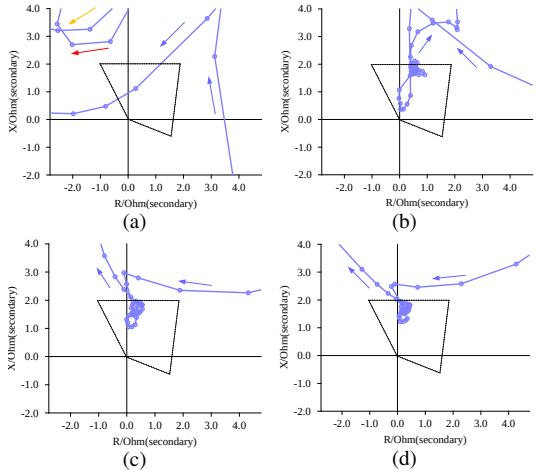

Fig. 18. Impedance plane for A–B fault at 75% of L1 in DK1: (a) T1, constant reactive power control. (b) T1, balanced current control. (c) T2, balanced current control. (d) T5, balanced current control.

farms are in operation. It is assumed that the control strategy of the VSC-HVDC station at bus EDR can be changed among constant active power, balanced current and constant reactive power control. The converter current limit is set to 1 p.u. and the reactive power reference is generated using the same assumption as described in Section IV. The whole system is modelled with details in RTDS.

For an A–B fault at different locations of L1, Fig. 17 summarizes the average response time of the relay under different VSC control strategies with various pre-fault system topologies of the examined area. Regarding T1 where the short circuit current seen by the relay is mainly provided by the VSC station, the relay has the slowest response and fails to trip when constant reactive power control is deployed. Figure 18(a)–(b) presents the impedance plane for A–B faults at 75% of L1 when constant reactive power and balanced current control are used. In Fig. 18(a), the locus still has discontinuous features similar to Fig. 7(d), leading to a refuse-to-trip failure. Once again, constant reactive power yields the worst relay performances. On the other hand, in T2–T5 where there are additional short circuit current contribution from SCDER, L2 or L3, the measured impedance locus has fewer transients (by comparing Fig. 18(c)–(d) to Fig. 18(b)) and the response time of the relay is improved. When the short circuit current is jointly provided by the VSC and synchronous sources (T2–T5), constant active power control yields slightly better performances than balanced current control in terms of the relay response time. However, constant reactive power control still leads to the longest response time of the distance relay compared to the other two control strategies. The test results on DK1 are similar to those from Section IV, which further verifies that the reliability of distance protection is correlated with the choice of VSC control strategies.

VI. Conclusions

With the converter current limit considered, this work investigates the impact of VSC control strategies and the incorporation of synchronous condensers on distance protection under unbalanced faults through HIL tests. The test results have shown that the reliability and speed of distance protection can be adversely affected due to a lower short circuit current level and non-conventional short circuit current characteristics, especially when the short circuit current is mainly contributed by VSCs. The application of a synchronous condenser at the PCC helps retain better relay performances under unbalanced faults, but this depends on the deployed VSC control strategies. Based on the test results, we propose to avoid the use of constant reactive power control together with distance relay. It can cause the relay to be unable to calculate the impedance accurately or can even lower the combined short circuit current when there is a synchronous condenser connected at the PCC, thus affecting the reliability of the relay. When the short circuit current is solely provided by a VSC, both constant active power and balanced current control can be considered for practice. When a synchronous condenser is connected at the PCC of a VSC, constant active power control can be considered for the VSC as it requires a smaller synchronous condenser than the other two control strategies to retain the relay performances.

References

[1] "Energy strategy 2050," The Danish Ministry of Climate and Energy, Copenhagen, Denmark, Feb. 2011.

[2] F. Blaabjerg, R. Teodorescu, M. Liserre, and A. V. Timbus, "Overview of control and grid synchronization for distributed power generation systems," *IEEE Trans. Ind. Electron.*, vol. 53, no. 5, pp. 1398–1409, Oct. 2006.

[3] H. Song and K. Nam, "Dual current control scheme for PWM converter under unbalanced input voltage conditions," *IEEE Trans. Ind. Electron.*, vol. 45, no. 5, pp. 953–959, Oct. 1998.

[4] A. Yazdani and R. Iravani, "A unified dynamic model and control for the voltage-sourced converter under unbalanced grid conditions," *IEEE Trans. Power Del.*, vol. 21, no. 3, pp. 1620–1629, Jul. 2006.

[5] S. Alepuz, S. Busquets-Monge, J. Bordonau, J. A. Martínez-Velasco, C. A. Silva, J. Pontt, and J. Rodríguez, "Control strategies based on symmetrical components for grid-connected converters under voltage dips," *IEEE Trans. Ind. Electron.*, vol. 56, no. 6, pp. 2162–2173, Jun. 2009.

[6] K. Ma, W. Chen, M. Liserre, and F. Blaabjerg, "Power controllability of a three-phase converter with an unbalanced AC source," *IEEE Trans. Power Electron.*, vol. 30, no. 3, pp. 1591–1604, Mar. 2015.

[7] R. Kabiri, D. G. Holmes, and B. P. McGrath, "Control of active and reactive power pipple to mitigate unbalanced grid voltages," *IEEE Trans. Ind. Appl.*, vol. 52, no. 2, pp. 1660–1668, Mar.–Apr. 2016.

[8] F. Wang, J. L. Duarte, and M. A. M. Hendrix, "Pliant active and reactive power control for grid-interactive converters under unbalanced voltage dips," *IEEE Trans. Power Electron.*, vol. 26, no. 5, pp. 1511–1521, May 2011.

[9] R. Teodorescu, M. Liserre, and P. Rodríguez, *Grid converters for photovoltaic and wind power systems*. Chichester, UK: John Wiley & Sons, Ltd., 2011.

[10] J. Miret, A. Camacho, M. Castilla, L. G. D. Vicuña, and J. Matas, "Control scheme with voltage support capability for distributed generation inverters under voltage sags," *IEEE Trans. Power Electron.*, vol. 28, no. 11, pp. 5252–5262, Nov. 2013.

[11] A. Camacho, M. Castilla, J. Miret, R. Guzman, and A. Borrell, "Reactive power control for distributed generation power plants to comply with voltage limits during grid faults," *IEEE Trans. Power Electron.*, vol. 29, no. 11, pp. 6224–6234, Nov. 2014.
[12] A. Milicua, G. Abad, and M. Á. R. Vidal, "Online reference limitation method of shunt-connected converters to the grid to avoid exceeding voltage and current limits under unbalanced operation part I: theory," *IEEE Trans. Energy Convers.*, vol. 30, no. 3, pp. 852–863, Sep. 2015.
[13] F. Nejabatkhah, Y. Li, and B. Wu, "Control strategies of three-phase distributed generation inverters for grid unbalanced," *IEEE Trans. Power Electron.*, vol. 31, no. 7, pp. 5228–5241, Jul. 2016.
[14] A. Camacho, M. Castilla, J. Miret, A. Borrell, and L. G. D. Vicuña, "Active and reactive power strategies with peak current limitation for distributed generation inverters during unbalanced grid faults," *IEEE Trans. Ind. Electron.*, vol. 62, no. 3, pp. 1515–1525, Mar. 2015.
[15] J. L. Sosa, M. Castilla, J. Miret, J. Matas, and Y. A. Al-Turki, "Control strategy to maximize the power capability of pv three-phase inverters during voltage sags," *IEEE Trans. Power Electron.*, vol. 31, no. 4, pp. 3314–3323, Apr. 2016.
[16] R. Li, C. Booth, A. Dyśko, A. Roscoe, J. Zhu, and H. Urdal, "Protection challenges in future converter dominated power systems," in *Proc. 6th Protection, Automation and Control World Conf.*, pp. 1–6, Glasgow, UK, Jun./Jul. 2015.
[17] S. M. Holder, L. Hang, and B. K. Johnson, "Investigation of transmission line protection performance in an electric grid with electronically coupled generation," in *Proc. North Amer. Power Symp.*, pp. 1–6, Manhatan, KS, USA, Sep. 2013.
[18] L. He, C. Liu, A. Pitto, and D. Cirio, "Distance protection of AC grid with HVDC-connected offshore wind generators," *IEEE Trans. Power Del.*, vol. 29, no. 2, pp. 493–501, Apr. 2014.
[19] A. Roy and B. K. Johnson, "Transmission side protection performance with Type-IV wind turbine system integration," in *Proc. North Amer. Power Symp.*, pp. 1–6, Pullman, Washington, USA, Sep. 2014.
[20] A. Hooshyar, M. A. Azzouz, and E. F. El-Saadany, "Distance protection of lines emanating from full-scale converter-interfaced renewable energy power plants part I: problem statement," *IEEE Trans. Power Del.*, vol. 30, no. 4, pp. 1770–1780, Aug. 2015.
[21] M. M. Alam, H. Leite, J. Liang, and A. D. S. Carvalho, "Effects of VSC based HVDC system on distance protection of transmission lines," *Int. J. of Elect. Power and Energy Syst.*, vol. 92, pp. 245–260, Nov. 2017.
[22] I. Erlich, T. Neumann, F. Shewarega, P. Schegner, and J. Meyer, "Wind turbine negative sequence current control and its effect on power system protection," in *Proc. IEEE PES General Meeting*, pp. 1–5, Denver, CO, USA, Jul. 2013.
[23] B. Chen, A. Shrestha, F. A. Ituzaro, and N. Fischer, "Addressing protection challenges associated with Type 3 and Type 4 wind turbine generators," in *Proc. 68th Annu. Conf. for Protective Relay Engineers*, pp. 335–344, College Station, TX, USA, Mar. 2015.
[24] M. M. Alam, H. Leite, N. Silva, and A. D. S. Carvalho, "Performance evaluation of distance protection of transmission lines connected with vsc-hvdc system using closed-loop test in rtds," *Electric Power Systems Research*, vol. 152, pp. 168 – 183, Nov. 2017.
[25] M. Nedd, Q. Hong, K. Bell, C. Booth, and P. Mohapatra, "Application of synchronous compensators in the gb transmission network to address protection challenges from increasing renewable generation," in *Proc. Cigre Study Committee B5 Colloq.*, pp. 1–6, Auckland, New Zealand, Sep. 2016.
[26] S. Kynev, G. Pilz, and H. Schmitt, "Comparison of modern statcom and synchronous condenser for power transmission systems," in *Proc. IEEE Elect. Power and Energy Conf.*, pp. 1–6, Ottawa, Canada, Oct. 2016.
[27] N. Masood, R. Yan, T. K. Saha, and S. Bartlett, "Post-retirement utilisation of synchronous generators to enhance security performances in a wind dominated power system," *IET Gener., Transm. Distrib.*, vol. 10, no. 13, pp. 3314–3321, Oct. 2016.
[28] Z. H. Rather, Z. Chen, P. Thøgersen, and P. Lund, "Dynamic reactive power compensation of large-scale wind integrated power system," *IEEE Trans. Power Syst.*, vol. 30, no. 5, pp. 2516–2526, Sep. 2015.
[29] E. Marrazi, G. Yang, and P. Weinreich-Jensen, "Allocation of synchronous condensers for restoration of system short-circuit power," *J. of Modern Power Syst. and Clean Energy*, vol. 6, no. 1, pp. 17–26, Jan. 2018.
[30] H. Akagi, E. H. Watanabe, and M. Aredes, *Instantaneous power theory and applications to power conditioning*. Hoboken, NJ, USA: John Wiley & Sons, Inc., 2006.
[31] The stable way–synchronous condenser solutions. (2017, Jul.). [Online]. Available: https://www.energy.siemens.com/hq/pool/hq/power-transmission/FACTS/Synchronous%20Condenser/Synchronous_Condenser.pdf
[32] *Technical Regulation 3.2.5 for Wind Power Plants With a Power Output Above 11 kW*, Energinet, Fredericia, Denmark, Jun. 2015.
[33] A. A. van der Meer, M. Ndreko, M. Gibescu, and M. A. M. M. van der Meijden, "The effect of frt behavior of vsc-hvdc-connected offshore wind power plants on ac/dc system dynamics," *IEEE Trans. Power Del.*, vol. 31, no. 2, pp. 878–887, Apr. 2016.
[34] S. H. Horowitz and A. G. Phadke, *Power system relaying, third edition*. Chichester, UK: John Wiley & Sons, Ltd., 2006.
[35] H. T. Nguyen, G. Yang, A. H. Nielsen, and P. H. Jensen, "Frequency stability improvement of low inertia systems using synchronous condensers," in *Proc. 2016 IEEE Int. Conf. on Smart Grid Commun.*, pp. 650–655, Sydney, NSW, Australia, Nov. 2016.

Jundi Jia received the B.Sc. degree in electrical engineering and automation from Beijing Jiaotong University, China, in 2012, and the M.Sc degree in electric power engineering from KTH Royal Institute of Technology, Stockholm, Sweden, in 2014.

In 2015, he was a strategy consulting analyst on resource utilities in Accenture, Beijing, China. Currently, he is pursuing Ph.D. degree in the Center for Electric Power and Energy, Technical University of Denmark, Kongens Lyngby, Denmark. In 2017, he was a visiting researcher in National Renewable Energy Laboratory (NREL), Colorado, USA. His research interests include power system dynamics and protection, power electronics and integration of renewable energy.

Guangya Yang received the B.E., M.E., and Ph.D. degrees all in the field of electric power system, in 2002, 2005, and 2008, respectively.

Since 2009, he has been with the Technical University of Denmark, Kongens Lyngby, Denmark, as a Postdoctoral Researcher, and he is currently an Associate Professor with the Center for Electric Power and Energy, Department of Electrical Engineering, Technical University of Denmark. Since 2009, he has been leading several industrial collaborative projects in Denmark in the field of monitoring, operation and protection of renewable energy systems. His research interests include renewable energy integration, smart grids, and cyber-physical energy systems.

Arne Hejde Nielsen is an Associate Professor at the Centre for Electric Power and Energy, Department of Electrical Engineering, Technical University of Denmark, Kongens Lyngby, Denmark. He has 30 years experience in electric power engineering; the first years were from ASEA AB, Central Research and Development Department, Sweden, with focus on measurement technology and motor design and control. Over the past decade, his focus has been on electric power systems, especially on the implementation of renewable energy sources in the power system.

Peter Rønne-Hansen received the M.Sc. degree in electrical engineering technologies from Technical University of Denmark, Kongens Lyngby, Denmark in 1991. He had various working experience as an electrical engineer in different companies, such as ELSAM Engineering, Vattenfall A/S, Denmark, and N1 A/S, Denmark. Currently, he is a protection engineer in Siemens A/S, Ballerup, Denmark. His interests includes power system protection and renewable energy integration.